

## **ANALYSIS OF ELECTROMAGNETIC SCATTERING WITH HIGHER-ORDER MOMENT METHOD AND NURBS MODEL**

**Z.-L. Liu**

Temasek Laboratories  
National University of Singapore  
117411, Singapore

**J. Yang**

School of Electrical and Electronic Engineering  
Nanyang Technological University  
639798, Singapore

**Abstract**—A novel scheme of combining non-uniform rational B-splines (NURBS) model with higher-order moment method (HOMM) is presented. The mesh precision of conforming to practical object is a major factor for HOMM to yield accurate results. In the present paper, NURBS technique is employed to model complex objects accurately with large curved Bezier patches and no factitious geometric discontinuities are introduced between the adjoining patches. The higher-order modified Legendre basis functions are defined on Bezier patch. As a result of the combination of NURBS model with HOMM, the accuracy of results is greatly improved compared with HOMM on curved parametric quadrilateral (CPQ) model, meanwhile, the number of unknowns is much reduced. Numerical results show that NURBS-HOMM is an efficient technique with good potential to solve the electromagnetic (EM) problems of complex electrically large objects.

### **1. INTRODUCTION**

The moment method (MM) is a powerful method to simulate many electromagnetic (EM) problems by discretizing the integral equations [1]. In traditional MM, the surfaces of 3D objects are divided into many flat triangle or quadrilateral elements, the size of which is

---

Corresponding author: Z.-L. Liu (tsliuz@nus.edu.sg).

on the order of  $\lambda/10$  in each dimension. Then the low order basis functions are defined on these elements, such as Rao-Wilton-Glisson (RWG) [2] and rooftop [3]. It seems to be a precise technique, but behind the scenes it's inherently inaccurate and must be tolerance dependent. When the electrical size of the object is large, a great number of elements and unknowns are required, and these lead to the cost of huge amount of memory and CPU time.

To reduce the computational cost, higher-order moment method (HOMM) is investigated [4–6]. Higher order polynomials basis functions are defined on curved parametric quadrilateral (CPQ) patches of arbitrary order [7], which are used to approximate the surfaces of 3D objects. The size of the CPQ patch is much larger than that of the traditional MM mesh, so the number of unknowns is decreased. However, the accuracy of the CPQ model is still not very good, even if the order of the patch is high. The factitious geometric discontinuities between the adjoining CPQ patches are unavoidable, because no tangential continuous conditions are considered when the CPQ model is built. So generating conformal mesh for HOMM is one of the major factors for the accuracy of results.

In recent years, the modeling technique of non-uniform rational B-splines (NURBS) is popular in computer aided geometric design (CAGD). It can conformally represent complex bodies very accurately, and no factitious geometric discontinuities are introduced because it's easy to meet the tangential continuous conditions by adjusting the control points and weights. In 1991, international standardization organization (ISO) published the standard for the exchange of product (STEP) model data (identified as ISO 10303) where NURBS was selected as the only mathematical method to define the shapes of industrial products [8]. It has been widely used in aircraft design, shipbuilding and other industries as the general format of model. And a lot of commercial softwares of computer aided design (CAD) support NURBS technique such as 3DMax, Maya, UG, etc. So if NURBS can be combined with computational electromagnetics (CEM), not only the accuracy will be improved, but also the application of CEM will be extended.

In the past several years, NURBS has been tried to apply to CEM. In 1994, Perez et al. analyzed the scattering characteristic of electrically large objects with physical optics (PO) and NURBS model [9, 10]. Then M. Domingo et al. introduced the RANURS code [11], which is based on PO+ECM (equivalent currents methods) and NURBS model. In 1997, the uniform theory of diffraction (UTD) was combined with NURBS surfaces to compute the radiation of onboard antennas [12]. In 2007, NURBS-UTD was used to solve radiation of antennas mounted

on complex platform [13].

As mentioned above, several CEM techniques have been well combined with NURBS model. However, most of them are high frequency methods (HFM). Compared to low frequency methods (LFM), HFM are easier to shift to NURBS surfaces, because only local characteristics of the surfaces are needed to consider, and no normal continuity and expansion accuracy of the current must be ensured. Although the hybrid MM-PO method with NURBS [14, 15] has been studied, triangle elements and RWG basis functions are still used in MM region, and NURBS surfaces are only for PO region. The true sense of combining MM with NURBS surfaces was proposed by L. Valle et al. [16], and the generalization of the planar rooftop basis functions are defined on Bezier patch. Actually, the advantage of NURBS model is not well taken by Valle in [16], because the size of patch can't be too large (the largest size is  $\lambda/4$ ). The limitation of the patch size is due to low order basis functions, and they can not approximate the surface current on large patch accurately. Another successful application of NURBS in CEM is combining characteristic basis function method (CBFM) with NURBS model [17, 18], and this technique is efficient in analyzing electrically large objects. So it's necessary and significant to study more applications of NURBS in CEM.

The higher-order basis functions can describe the surface current on large patch accurately and the NURBS model can well fit the complex object conformally with large curved patches. So, in this paper, we propose to combine NURBS model with higher-order basis functions to take full advantages of them. In the authors' opinion, NURBS model is a good and necessary choice for HOMM, which may be an efficient way to handle the EM problems of complex electrically large objects.

This paper is organized as follows. In Section 2, the definitions NURBS and Bezier patch are introduced, and the modified expression of Bezier patch is deduced to meet the requirement of HOMM. Section 3 presents the methodology of combining NURBS model with HOMM in detail and gives the matrix equation. Some representative results are illustrated in Section 4 to show the advantage and efficiency of NURBS-HOMM. Finally, we give the conclusions in Section 5 to close the paper.

## 2. DEFINITION OF NURBS MODEL

This section includes two parts. Firstly, the knowledge of NURBS and Bezier patch is presented; secondly, the modified expression of Bezier patch is deduced so that the higher-order basis functions can be defined

on Bezier patch.

## 2.1. NURBS and Bezier Patch

The expression of NURBS surface is illustrated as follows [19]

$$\vec{r}(\bar{u}, \bar{v}) = \frac{\sum_{i=0}^m \sum_{j=0}^n w_{ij} \vec{P}_{ij} N_i^p(\bar{u}) N_j^q(\bar{v})}{\sum_{i=0}^m \sum_{j=0}^n w_{ij} N_i^p(\bar{u}) N_j^q(\bar{v})}, \quad \bar{u}, \bar{v} \in [0, 1], \quad (1)$$

where  $\vec{P}_{ij}$  are the control points,  $w_{ij}$  are the weights, and  $N_i^p(t)$  are the normalized B-spline basis functions of degree  $p$  defined recursively as [20, 21]

$$N_i^0(t) = \begin{cases} 1, & t_i \leq t \leq t_{i+1} \\ 0, & \text{otherwise} \end{cases}, \quad (2)$$

$$N_i^p(t) = \frac{t - t_i}{t_{i+p} - t_i} N_i^{p-1}(t) + \frac{t_{i+p+1} - t}{t_{i+p+1} - t_{i+1}} N_{i+1}^{p-1}(t), \quad (3)$$

where  $t_i$  are the so-called knots which form a knot vector  $T = \{t_0, t_1, \dots, t_{m+p+1}\}$ .

Before applying NURBS to CEM, NURBS surface is needed to transform to Bezier format. The underlying reason why a transformation is required is the lack of simple numerically stable algorithms for determining derivatives for NURB-splines. The transformation is convenient to implement by using Cox-De Boor algorithm [22].

Bezier patch is defined by the degrees, a set of control points and weight values, as shown in Figure 1, and expressed in the following

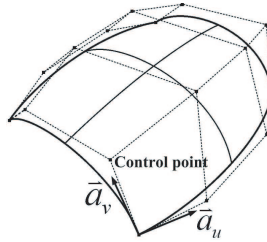


**Figure 1.** A Bezier patch. The control points and the  $u$ - $v$  coordinates are displayed.

way

$$\vec{r}(\bar{u}, \bar{v}) = \frac{\sum_{i=0}^m \sum_{j=0}^n w_{ij} \vec{P}_{ij} B_i^m(\bar{u}) B_j^n(\bar{v})}{\sum_{i=0}^m \sum_{j=0}^n w_{ij} B_i^m(\bar{u}) B_j^n(\bar{v})}, \quad \bar{u}, \bar{v} \in [0, 1], \quad (4)$$

where  $\vec{P}_{ij}$  are the control points,  $w_{ij}$  are the weights, and  $B_i^m(t)$  are the Bernstein polynomials of degree  $m$  defined as

$$B_i^m(t) = \frac{m!}{i!(m-i)!} t^i (1-t)^{m-i}, \quad (5)$$

where  $t \in [0, 1]$ , and for mathematical convenience  $B_i^m(t) = 0$  if  $i \notin \{0, 1, \dots, m\}$ .

## 2.2. Modified Expression of Bezier Patch

As shown in (4), the parameters of Bezier patch  $\bar{u}$  and  $\bar{v}$  are limited within  $[0, 1]$ . However, higher-order modified Legendre basis functions are defined on  $[-1, 1]$ , so Eq. (4) must be modified to meet the requirement of the basis functions. We now introduce the new parameters  $u$  and  $v$  defined as

$$\begin{cases} u = 2\bar{u} - 1 \\ v = 2\bar{v} - 1 \end{cases}. \quad (6)$$

So  $u, v \in [-1, 1]$ , and the expression of Bezier patch can be written in terms of  $u$  and  $v$  as

$$\vec{r}(u, v) = \frac{\sum_{i=0}^m \sum_{j=0}^n w_{ij} \vec{P}_{ij} B_i^m(0.5u + 0.5) B_j^n(0.5v + 0.5)}{\sum_{i=0}^m \sum_{j=0}^n w_{ij} B_i^m(0.5u + 0.5) B_j^n(0.5v + 0.5)}. \quad (7)$$

## 3. HIGHER-ORDER MOMENT METHOD FORMULATION ON BEZIER PATCH

In this section, the integral equation for conducting scatter is introduced first. To solve the integral equation, NURBS model and HOMM are employed, and the definitions of higher-order modified Legendre basis functions on Bezier patch and testing functions are described. Finally, the impedance matrix terms of MM are derived.

### 3.1. Integral Equation Formulation

Consider the surface  $S$  of an open or closed perfectly electrically conducting (PEC) scatter with unit normal  $\hat{n}$ . Let  $\vec{E}^i$  denote the impressed electric field on surface  $S$ .  $\vec{J}_S$  is the surface current density induced by  $\vec{E}^i$ , and they satisfy the electric field integral equation (EFIE) on surface  $S$

$$\hat{n} \times \vec{E}^i = \hat{n} \times \left[ j\omega\mu \int_S \vec{J}_S(\vec{r}') G(\vec{r}', \vec{r}) dS' - \frac{1}{j\omega\varepsilon} \nabla \int_S \nabla'_S \cdot \vec{J}_S(\vec{r}') G(\vec{r}', \vec{r}) dS' \right], \quad (8)$$

where  $G(\vec{r}', \vec{r})$  is the Green's function in free space defined as

$$G(\vec{r}', \vec{r}) = \frac{e^{-jk|\vec{r} - \vec{r}'|}}{4\pi|\vec{r} - \vec{r}'|}, \quad (9)$$

$k = \omega\sqrt{\varepsilon\mu} = 2\pi/\lambda$  is the wavenumber, and  $\vec{r}'$  and  $\vec{r}$  are the source and observation points, respectively.

### 3.2. Basis Functions on Bezier Patch

NURBS model is transformed to Bezier patches before combined with HOMM, and the higher-order modified Legendre basis functions [7] are defined on Bezier patch. For the definition domain of basis functions is  $[-1, 1]$ , Eq. (7), the modified expression of Bezier patch, is used. Consider a PEC surface which is divided into  $Q$  Bezier patches of arbitrary order, as shown in Figure 2.

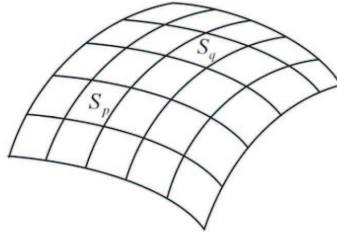


**Figure 2.** A PEC surface is divided into  $Q$  Bezier patches of arbitrary order.

The surface current density  $\vec{J}_S$  on each patch is described in terms of the contravariant components as

$$\vec{J}_S(\vec{r}) = \vec{J}_S^u(\vec{r}) \vec{a}_u + \vec{J}_S^v(\vec{r}) \vec{a}_v, \quad (10)$$

where  $\vec{a}_u$  and  $\vec{a}_v$  are the covariant unitary vectors given by

$$\vec{a}_u = \frac{\partial \vec{r}}{\partial u}, \quad (11a)$$

$$\vec{a}_v = \frac{\partial \vec{r}}{\partial v}. \quad (11b)$$

The two components  $J_S^u(\vec{r})$  and  $J_S^v(\vec{r})$  are expanded as

$$J_S^u(\vec{r}) = J_S^u(u, v) = \frac{1}{Ja(u, v)} \sum_{m=0}^M \sum_{n=0}^N b_{mn}^u f_{mn}^u(u, v), \quad (12a)$$

$$J_S^v(\vec{r}) = J_S^v(u, v) = \frac{1}{Ja(u, v)} \sum_{m=0}^M \sum_{n=0}^N b_{mn}^v f_{mn}^v(u, v), \quad (12b)$$

where  $b_{mn}^u$  and  $b_{mn}^v$  are the unknown coefficients, and  $Ja(u, v) = |\vec{a}_u \times \vec{a}_v|$  is the surface Jacobian.  $f_{mn}^u(u, v)$  and  $f_{mn}^v(u, v)$  are the higher-order modified Legendre basis functions defined as

$$f_{mn}^u(u, v) = \tilde{P}_m(u) P_n(v), \quad (13a)$$

$$f_{mn}^v(u, v) = \tilde{P}_m(v) P_n(u), \quad (13b)$$

where  $P_m(u)$  and  $\tilde{P}_m(u)$  are, respectively, Legendre polynomials and modified Legendre polynomials expressed as

$$P_m(u) = \frac{1}{2^m m!} \frac{d^m}{du^m} (u^2 - 1)^m, \quad (14a)$$

$$\tilde{P}_m(u) = \begin{cases} 1 - u, & m = 0 \\ 1 + u, & m = 1 \\ P_m(u) - P_{m-2}(u), & m \geq 2. \end{cases} \quad (14b)$$

The normal component of the surface current density is continuous across the common edge, and the detailed discussion can be found in [7].

### 3.3. Matrix Equation Derivation

The Galerkin testing procedure is employed, and the testing functions are represented as

$$\vec{w}_{st}^u(\vec{r}) = \frac{1}{Ja(u, v)} f_{st}^u(u, v) \vec{a}_u, \quad (15a)$$

$$\vec{w}_{st}^v(\vec{r}) = \frac{1}{Ja(u, v)} f_{st}^v(u, v) \vec{a}_v. \quad (15b)$$

With  $S_p$  and  $S_q$  being the observation and source patches, respectively, the whole surface can be expressed as (Figure 2)

$$S = \sum_{p=1}^Q S_p = \sum_{q=1}^Q S_q. \quad (16)$$

The subscripts  $p$  and  $q$  hereafter are used to denote the observation and source patches.

Equation (8) is tested with (15a), yielding

$$\begin{aligned} \int_{S_p} \vec{w}_{st,p}^u \cdot \vec{E}^i(\vec{r}) dS_p &= j\omega\mu \int_{S_p} \vec{w}_{st,p}^u \cdot \int_S \vec{J}_S(\vec{r}') G(\vec{r}', \vec{r}) dS' dS_p \\ &- \frac{1}{j\omega\varepsilon} \int_{S_p} \vec{w}_{st,p}^u \cdot \nabla_S \int_S \nabla'_S \cdot \vec{J}_S(\vec{r}') G(\vec{r}', \vec{r}) dS' dS_p. \end{aligned} \quad (17)$$

In derivation, the vector calculus identity  $\nabla \cdot (f \vec{a}) = f \nabla \cdot \vec{a} + \vec{a} \cdot \nabla f$  [23] is used to transfer the surface gradient operator  $\nabla_S$  to the testing function, and the second item of the right side of (17) can be rewritten as

$$\begin{aligned} &\int_{S_p} \vec{w}_{st,p}^u \cdot \nabla_S \int_S \nabla'_S \cdot \vec{J}_S(\vec{r}') G(\vec{r}', \vec{r}) dS' dS_p \\ &= - \int_{S_p} \nabla_S \cdot \vec{w}_{st,p}^u \int_S \nabla'_S \cdot \vec{J}_S(\vec{r}') G(\vec{r}', \vec{r}) dS' dS_p. \end{aligned} \quad (18)$$

Substitute (18) into (17), we obtain

$$\begin{aligned} \int_{S_p} \vec{w}_{st,p}^u \cdot \vec{E}^i(\vec{r}) dS_p &= j\omega\mu \int_{S_p} \vec{w}_{st,p}^u \cdot \int_S \vec{J}_S(\vec{r}') G(\vec{r}', \vec{r}) dS' dS_p \\ &+ \frac{1}{j\omega\varepsilon} \int_{S_p} \nabla_S \cdot \vec{w}_{st,p}^u \int_S \nabla'_S \cdot \vec{J}_S(\vec{r}') G(\vec{r}', \vec{r}) dS' dS_p. \end{aligned} \quad (19)$$

The surface divergence of the testing functions and the surface current density can be written as

$$\nabla_S \cdot \vec{w}_{st,p}^u = \frac{1}{J a_p(u, v)} \frac{\partial f_{st,p}^u(u, v)}{\partial u}, \quad (20a)$$

$$\nabla_S \cdot \vec{w}_{st,p}^v = \frac{1}{J a_p(u, v)} \frac{\partial f_{st,p}^v(u, v)}{\partial v}, \quad (20b)$$

$$\begin{aligned} \nabla'_S \cdot \vec{J}_S(\vec{r}'_q) &= \frac{1}{J a_q(u', v')} \cdot \left[ \sum_{m=0}^M \sum_{n=0}^N b_{mn,q}^u \frac{\partial f_{mn,q}^u(u', v')}{\partial u'} \right. \\ &\quad \left. + \sum_{m=0}^M \sum_{n=0}^N b_{mn,q}^v \frac{\partial f_{mn,q}^v(u', v')}{\partial v'} \right]. \end{aligned} \quad (21)$$

Substituting (10), (15a), (20a), and (21) into (19), and considering  $dS = J a(u, v) dudv$ , yield

$$\begin{aligned} \int_{S_p} f_{st,p}^u(u, v) \vec{a}_{u,p} \cdot \vec{E}^i(\vec{r}) dudv &= \sum_{q=1}^Q \left\{ \right. \\ &\sum_{m=0}^M \sum_{n=0}^N b_{mn,q}^u \int_{S_p} \int_{S_q} \left[ j\omega\mu f_{st,p}^u(u, v) f_{mn,q}^u(u', v') \vec{a}_{u,p} \cdot \vec{a}_{u,q} \right. \\ &+ \left. \frac{1}{j\omega\varepsilon} \frac{\partial f_{st,p}^u(u, v)}{\partial u} \frac{\partial f_{mn,q}^u(u', v')}{\partial u'} \right] G(\vec{r}_p, \vec{r}'_q) du' dv' dudv \\ &+ \sum_{m=0}^M \sum_{n=0}^N b_{mn,q}^v \int_{S_p} \int_{S_q} \left[ j\omega\mu f_{st,p}^v(u, v) f_{mn,q}^v(u', v') \vec{a}_{u,p} \cdot \vec{a}_{v,q} \right. \\ &+ \left. \frac{1}{j\omega\varepsilon} \frac{\partial f_{st,p}^v(u, v)}{\partial v} \frac{\partial f_{mn,q}^v(u', v')}{\partial v'} \right] G(\vec{r}_p, \vec{r}'_q) du' dv' dudv \left. \right\} \quad (22) \end{aligned}$$

When  $p, q = 1, 2, \dots, Q$ , Eq. (22) can be expressed in matrix form as

$$[V_{st}^u]_p = \begin{bmatrix} [Z_{st,mn}^{uu}]_{pq} & [Z_{st,mn}^{uv}]_{pq} \end{bmatrix} \begin{bmatrix} [b_{mn}^u]_q \\ [b_{mn}^v]_q \end{bmatrix}. \quad (23)$$

where  $[V_{st}^u]_p$ ,  $[Z_{st,mn}^{uu}]_{pq}$ ,  $[Z_{st,mn}^{uv}]_{pq}$ ,  $[b_{mn}^u]_q$  and  $[b_{mn}^v]_q$  are submatrixes for each value(s) of  $p$  and/or  $q$ . Elements of  $[V_{st}^u]_p$ ,  $[Z_{st,mn}^{uu}]_{pq}$ ,  $[Z_{st,mn}^{uv}]_{pq}$

are given by

$$V_{st,p}^u = \int_{S_p} f_{st,p}^u(u, v) \vec{a}_{u,p} \cdot \vec{E}^i(\vec{r}) dudv, \quad (24)$$

$$Z_{st,mn,pq}^{uu} = \int_{S_p} \int_{S_q} \left[ j\omega\mu f_{st,p}^u(u, v) f_{mn,q}^u(u', v') \vec{a}_{u,p} \cdot \vec{a}_{u,q} \right. \\ \left. + \frac{1}{j\omega\varepsilon} \frac{\partial f_{st,p}^u(u, v)}{\partial u} \frac{\partial f_{mn,q}^u(u', v')}{\partial u'} \right] G(\vec{r}_p, \vec{r}'_q) du' dv' dudv, \quad (25)$$

$$Z_{st,mn,pq}^{uv} = \int_{S_p} \int_{S_q} \left[ j\omega\mu f_{st,p}^u(u, v) f_{mn,q}^v(u', v') \vec{a}_{u,p} \cdot \vec{a}_{v,q} \right. \\ \left. + \frac{1}{j\omega\varepsilon} \frac{\partial f_{st,p}^u(u, v)}{\partial u} \frac{\partial f_{mn,q}^v(u', v')}{\partial v'} \right] G(\vec{r}_p, \vec{r}'_q) du' dv' dudv. \quad (26)$$

Similarly, Eq. (8) is tested with (15b), we can obtain another matrix equation

$$[V_{st}^v]_p = \begin{bmatrix} [Z_{st,mn}^{vu}]_{pq} & [Z_{st,mn}^{vv}]_{pq} \end{bmatrix} \begin{bmatrix} [b_{mn}^u]_q \\ [b_{mn}^v]_q \end{bmatrix}. \quad (27)$$

Combine (23) with (27), we get the matrix equation of NURBS-HOMM

$$\begin{bmatrix} [V_{st}^u]_p \\ [V_{st}^v]_p \end{bmatrix} = \begin{bmatrix} [Z_{st,mn}^{uu}]_{pq} & [Z_{st,mn}^{uv}]_{pq} \\ [Z_{st,mn}^{vu}]_{pq} & [Z_{st,mn}^{vv}]_{pq} \end{bmatrix} \begin{bmatrix} [b_{mn}^u]_q \\ [b_{mn}^v]_q \end{bmatrix}. \quad (28)$$

The general form of (28) is  $[V] = [Z][b]$ , and  $[V]$ ,  $[Z]$  and  $[b]$  are in block form. The unknown coefficients  $[b]$  can be obtained by solving the matrix Equation (28).

When  $p = q$ , the observation and source points are on the same patch, and we have to solve the singularity of self-term matrix element. A purely numerical annihilation procedure based on the Duffy transform [24] is used in this paper, which has been applied to hexahedrals by Sertel and Volakis [25], and the details can be found in [7].

#### 4. NUMERICAL RESULTS

In this section, three example will be illustrated, and bistatic RCS obtained by NURBS-HOMM will be given. As comparison, the results of HOMM on first order (bilinear) and second order (biquadratic) CPQ model, Mie's series (example 1), RWG (example 2), and fast multiple

method (FMM) (example 3) are given, and the meshes of NURBS models and bilinear quadrilaterals models (first order CPQ model) are also displayed. The root-mean-square (RMS) error of the RCS is used to describe the accuracy of results, and it's defined as

$$\text{RMS} = \sqrt{\frac{1}{N_s} \sum_{i=1}^{N_s} |\sigma_{\text{HOMM}} - \sigma_0|^2} \quad (29)$$

where  $N_s$  is the number of bistatic observing points,  $\sigma_{\text{HOMM}}$  is RCS in dB calculated by HOMM, and  $\sigma_0$  is that calculated by Mie's series, RWG and FMM in the three example, respectively. All examples run on a PC of 1.86 GHz intel processor with 2 GB RAM.

#### 4.1. PEC Sphere

The first example is a PEC sphere of radius 1 wavelength. The meshes of NURBS and first order CPQ models consist of (a) 16 Bezier patches and (b) 54 bilinear quadrilaterals are shown in Figure 3. Figure 4 plots the bistatic RCS of the sphere. The details of the orders of basis functions, the numbers of patches and unknowns, and RMS errors are list in Table 1. Obviously, NURBS-HOMM, needs fewer unknowns, but gives more accurate result than the CPQ model compared with Mie's series solution.

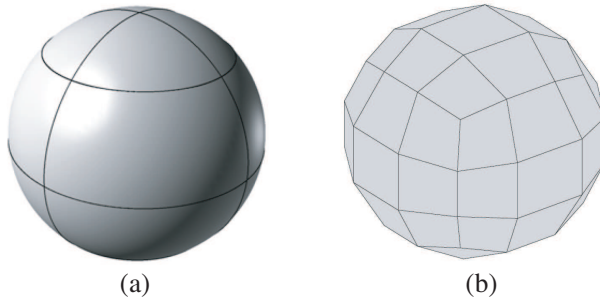


**Figure 3.** Sphere models consist of (a) 16 Bezier patches and (b) 54 bilinear quadrilaterals.

#### 4.2. PEC Horn

Figure 5 shows a PEC horn modeled by (a) NURBS and (b) bilinear quadrilaterals. The direction of the  $E_x$ -polarized incident plane wave is  $\theta = 0^\circ$ ,  $\varphi = 0^\circ$ . Figure 6 plots the bistatic RCS in  $\varphi = 0^\circ$  plane and

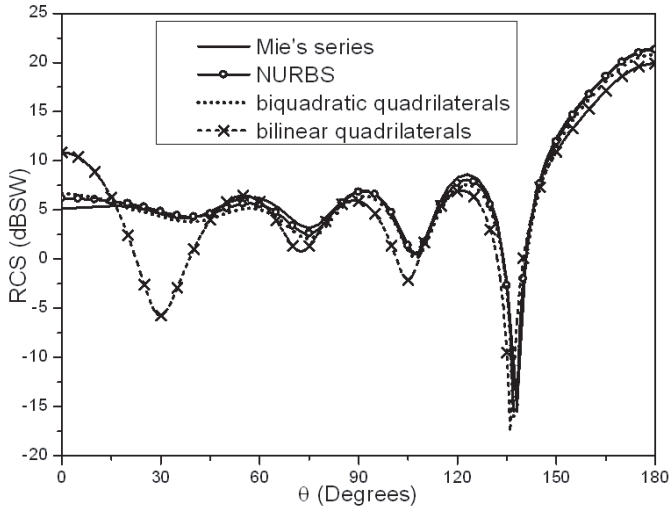


**Figure 4.** Bistatic RCS of the sphere and the radius is 1 wavelength.

**Table 1.** The basis functions orders, number of patches and unknowns, CPU time, and RMS error for PEC sphere.

	Orders of basis functions	Number of patches	Number of unknowns	CPU time (s)	RMS error (dB)
NURBS	$M = 3, N = 2$	16	276	61	0.451
biquadratic	$M = 3, N = 2$	24	432	227	0.830
bilinear	$M = 3, N = 2$	54	972	107	3.511

sweeping  $\theta$  from  $0^\circ$  to  $180^\circ$  obtained from NURBS-HOMM and HOMM with first and second order CPQ models compared with RWG solution. The orders of basis functions, the numbers of patches and unknowns, RMS errors for NURBS, CPQ models are illustrated in Table 2. With the same orders of basis functions, the result from NURBS model is more accurate than that from CPQ models, and much fewer patches and unknowns are needed by NURBS model than by CPQ models.

### 4.3. Aircraft-like Geometry

The last example is a PEC aircraft-like geometry modeled with (a) 176 Bezier patches and (b) 550 bilinear quadrilaterals, as shown in Figure 7. The working frequency is 600 MHz. The length and wingspan of the geometry is about  $12.86\lambda$  and  $15.71\lambda$ , respectively. The surface area of

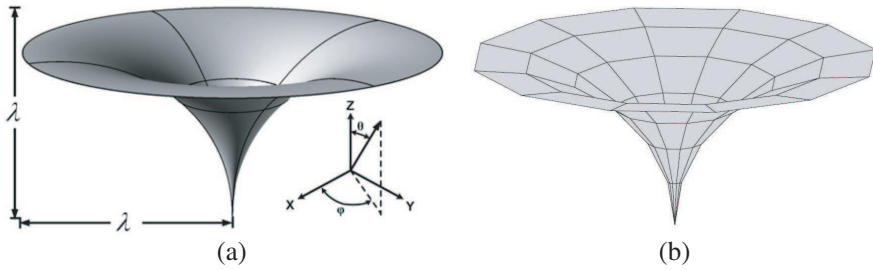


**Figure 5.** Horn models consist of (a) 8 Bezier patches and (b) 72 bilinear quadrilaterals.

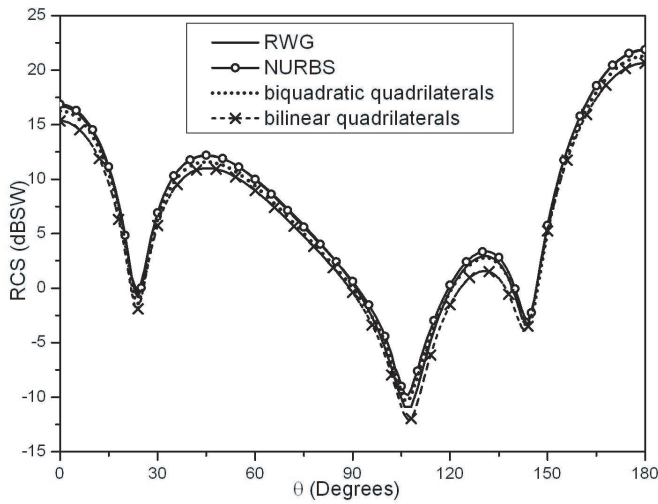


**Figure 6.** Bistatic RCS of the PEC horn.

**Table 2.** The basis orders, number of patches and unknowns, CPU time, and RMS error for PEC horn.

	Orders of basis functions	Number of patches	Number of unknowns	CPU time (s)	RMS error (dB)
NURBS	$M = 3, N = 2$	8	132	20	0.477
biquadratic	$M = 3, N = 2$	18	306	106	0.556
bilinear	$M = 3, N = 2$	72	1458	228	1.128
RWG	$n/a$	1276	1877	78	0

the aircraft is about  $184.53\lambda^2$ . The direction of the incident plane wave is  $\theta = 90^\circ$ ,  $\varphi = 45^\circ$ , and the polarization is  $E_\varphi$ . Figure 8 displays the results of bistatic RCS in  $xoy$  plane obtained from NURBS-HOMM and HOMM on first order CPQ model. For comparison, the result of FMM with RWG and Galerkin testing is also given in the Figure. Table 3 shows the basis functions orders, numbers of patches and unknowns, and RMS errors.

**Table 3.** The basis orders, number of patches and unknowns, CPU time, and RMS error for PEC aircraft.

	Orders of basis functions	Number of patches	Number of unknowns	CPU time (s)	RMS error (dB)
NURBS	$M = 3, N = 2$	176	3000	5081	2.365
bilinear 1	$M = 3, N = 2$	550	9366	8706	4.373
bilinear 2	$M = 5, N = 4$	550	26610	10360	3.862
FMM	$n/a$	25105	37655	2143	0

When the orders of basis functions are  $M = 3$  and  $N = 2$ , NURBS-HOMM gives the result which agrees well with FMM solution, and only 176 Bezier patches and 3000 unknowns are needed. Compared with NURBS-HOMM, HOMM on CPQ model can just give the very rough result (bilinear 1), while more than 3 times numbers of patches and unknowns are required. Then we increase the basis functions orders of HOMM on CPQ model and let  $M = 5, N = 4$ , which results in 26610 unknowns. But the obtained result (bilinear 2) is still less accurate

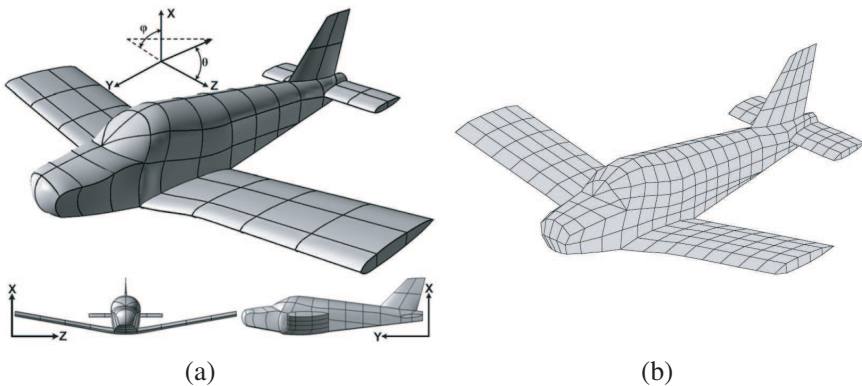


**Figure 7.** Aircraft models consist of (a) 176 Bezier patches and (b) 550 bilinear quadrilaterals.

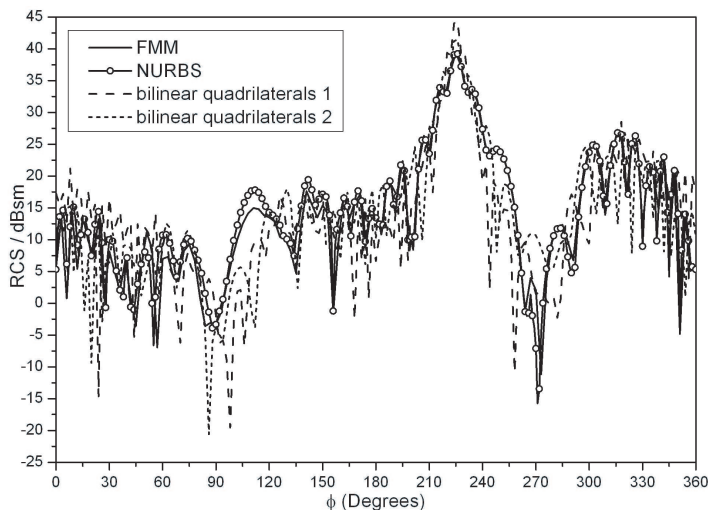


**Figure 8.** Bistatic RCS of the aircraft.

than that of NURBS-HOMM. Combining NURBS with HOMM can much reduce the number of unknowns and improve the accuracy of the result because NURBS model can describe the arbitrary object more accurately than CPQ model with fewer curved patches as described in Figure 7. Even if HOMM with CPQ model employs higher basis functions orders, it still can not provide result of good accuracy.

The mesh precision of conforming to practical object is a major factor for HOMM to yield accurate results. For simple geometries, the accuracy of CPQ model is as same as that of NURBS model, such as the results of second order (biquadratic) CPQ model in example 1 and 2. Actually, sphere and horn are quadratic surfaces in differential geometry, which have their corresponding second degree expressions  $x^2 + y^2 + z^2 = 1$  and  $\{z = \sqrt{1 - (1 - \sqrt{x^2 + y^2})^2}, x^2 + y^2 \leq 1\}$ . The second order CPQ model is just another form of expressions in the local coordinates of each patch. For flat plate and polyhedron, first order CPQ model also has the same accuracy with NURBS model. However, practical objects always have arbitrary shapes; they are complex and usually we can't find expressions for them, such as example 3. For these cases, CPQ model is not accurate enough, while NURBS can conformally represent complex curved surfaces very well, and no factitious geometric discontinuities are introduced by adjusting the control points and weights to meet the tangential continuous conditions.

## 5. CONCLUSION

A new scheme that combines NURBS model with HOMM has been presented. Good quality conformal mesh is a major factor for HOMM to yield accurate results. NURBS is capable to describe complex objects conformally with much larger curved patches than bilinear quadrilaterals, and no factitious geometric discontinuities are introduced between adjoining patches. So combining NURBS with HOMM can greatly improve the accuracy of results compared with HOMM on CPQ model, meanwhile, the number of unknowns is much reduced. Numerical results show that NURBS-HOMM gives more accurate results than HOMM on CPQ model and reduces the number of unknowns by 60–90%. Therefore, NURBS-HOMM is an efficient technique which has good potential to solve the EM problems of complex electrically large objects.

## REFERENCES

1. Harrington, R. F., *Field Computation by Moment Methods*, Macmillan, New York, 1968.
2. Rao, S. M., D. R. Wilton, and A. W. Glisson, "Electromagnetic scattering by surfaces of arbitrary shape," *IEEE Trans. Antennas Propagat.*, Vol. 30, 409–418, May 1982.
3. Glisson, W. and D. R. Wilton, "Simple and efficient numerical methods for problems of electromagnetic radiation and scattering from surfaces," *IEEE Trans. Antennas Propagat.*, Vol. 28, 593–603, Sep. 1980.
4. Notaros, M., B. D. Popovic, J. P. Weem, et al., "Efficient large-domain MoM solutions to electrically large practical EM problems," *IEEE Trans. Microw. Theory and Techniques*, Vol. 49, 151–159, Jan. 2001.
5. Djordjevic, M. and B. M. Notaros, "Double higher order method of moments for surface integral equation modeling of metallic and dielectric antennas and scatterers," *IEEE Trans. Antennas Propagat.*, Vol. 52, 2118–2129, Aug. 2004.
6. Djordjevic, M. and B. M. Notaros, "Higher-order hierarchical basis functions with improved orthogonality properties for moment-method modeling of metallic and dielectric microwave structures," *Microw. Opt. Technol. Lett.*, Vol. 37, 83–88, Apr. 2003.
7. Jørgensen, E., J. L. Volakis, P. Meincke, and O. Breinbjerg, "Higher order hierarchical legendre basis functions for electro-

- magnetic modeling,” *IEEE Trans. Antennas Propagat.*, Vol. 52, 2985–2995, Nov. 2004.
8. Vergeest, J. S. M., “CAD surface data exchange using STEP,” *Computer-Aided Design*, Vol. 23, 269–281, May 1991.
  9. Perez, J. and M. F. Catedra, “RCS of electrically large targets modeled with NURBS surfaces,” *Electronics Letters*, Vol. 28, 1119–1121, Jun. 1992.
  10. Perez, J. and M. F. Catedra, “Application of physical optics to the RCS computation of bodies modeled with NURBS surfaces,” *IEEE Trans. Antennas Propagat.*, Vol. 42, 1404–1411, Oct. 1994.
  11. Domingo, M., F. Rivas, J. Perez, et al., “Computation of the RCS of complex bodies modeled using NURBS surfaces,” *IEEE Antennas and Propagat. Magazine*, Vol. 37, 36–47, Jun. 1995.
  12. Perez, J., J. A. Saiz, O. M. Conde, et al., “Analysis of antennas on board arbitrary structures modeled by NURBS surfaces,” *IEEE Trans. Antennas Propagat.*, Vol. 45, 1045–1053, Jun. 1997.
  13. Wang, N., C. H. Liang, and H. B. Yuan, “Calculation of pattern in UTD method based on NURBS modeling with the source on surface,” *Opt. Technol. Lett.*, Vol. 49, 2492–2498, Oct. 2007.
  14. Sefi, S., “Ray tracing tools for high frequency electromagnetics simulations,” Licentiate thesis, Royal Institute of Technology of Stockholm, Sweden, May 2003.
  15. Chen, M., Y. Zhang, X. W. Zhao, and C. H. Liang, “Analysis of antenna around nurbs surface with hybrid MoM-PO technique,” *IEEE Trans. Antennas Propagat.*, Vol. 55, 407–413, Feb. 2007.
  16. Valle, L., F. Rivas, and M. F. Catedra, “Combining the moment method with geometrical modeling by NURBS surfaces and Bezier patches,” *IEEE Trans. Antennas Propagat.*, Vol. 42, 373–381, Mar. 1994.
  17. Delgado, C., M. F. Catedra, and R. Mittra, “Application of the characteristic basis function method utilizing a class of basis and testing functions defined on NURBS patches,” *IEEE Trans. Antennas Propagat.*, Vol. 56, 784–791, Mar. 2008.
  18. Garcia, E., C. Delgado, I. G. Diego, and M. F. Catedra, “An iterative solution for electrically large problems combining the characteristic basis function method and the multilevel fast multipole algorithm,” *IEEE Trans. Antennas Propagat.*, Vol. 56, 2363–2371, Aug. 2008.
  19. Piegl, L., “On NURBS: A survey,” *IEEE Computer Graphics and Application*, Vol. 11, No. 1, 55–71, South Florida, 1991.
  20. De Boor, C., “On calculating with B-splines,” *Journal of*

- Approximation Theory*, Vol. 6, 50–62, Jul. 1972.
21. Cox, M. G., “The numerical evaluation of B-splines,” *IMA Journal of Applied Mathematics*, Vol. 10, 134–149, 1972.
  22. Boehm, W., “Inserting new knots into B-spline curves,” *Computer-Aided Design*, Vol. 12, 199–201, Jul. 1980.
  23. Van Bladel, J., *Electromagnetic Fields*, McGraw-Hill, New York, USA, 1964.
  24. Duffy, M. G., “Quadrature over a pyramid or cube of integrands with a singularity at a vertex,” *SIAM J. Numer. Anal.*, Vol. 19, 1260–1262, Dec. 1982.
  25. Sertel, K. and J. L. Volakis, “Method of moments solution of volume integral equations using parametric geometry,” *Radio Science*, Vol. 37, 1–7, Jan.–Feb. 2002.